Indian J Phys (November 2023) 97(13):4017–4029
https://doi.org/10.1007/s12648-023-02729-5

ORIGINAL PAPER

Stochastic resonance in an asymmetric tri-stable system driven by correlated noises and periodic signal

L He[1], X Liu[1]* and Z Jiang[2]

[1]School of Communication and Information Engineering, Chongqing University of Posts and Telecommunications, Chongqing 400065, China

[2]Cyberspace Administration of Guizhou Province, Guiyang 550000, China

Received: 11 March 2022 / Accepted: 11 April 2023 / Published online: 17 May 2023

Abstract: This paper proposes an Asymmetric Tri-stable Stochastic Resonance (ATSSR) system that is driven by a periodic signal and a combination of correlated non-Gaussian noise and Gaussian white noise. The authors obtain the Markov process using the unified color noise approximation method and derive analytical expressions for the steady-state probability density, the Mean First-Pass Time, and the spectral amplification under the adiabatic approximation limit. Afterwards, the effects of various system parameters on them are analyzed, and the results show that both non-Gaussian noise and Gaussian white noise can induce stochastic resonance, with stronger resonance occurring when the two types of noise are correlated. Then, a periodic attenuated pulse signal and a harmonic vibration signal are constructed, which are applied in simulated experiments to detect fault signals using the ATSSR system. The experimental results demonstrate the outstanding performances in detecting fault signals and confirm its the feasibility for this purpose.

Keywords: Stochastic resonance; Asymmetric tri-stable potential; Correlated noises; SA

1. Introduction

Over the past few decades, significant advancements have been made by scholars in the research of stochastic resonance (SR) [1], which has found widespread applications in various fields such as biological [2, 3], physical [4, 5], and neural networks [6, 7]. Initially, the focus of scholars was on SR in bistable systems that were driven by Gaussian white noise and periodic force. In Ref. [8], a second-order underdamped bistable system was proposed, which was driven by additive noise in the form of Gaussian white noise. Ref. [9] and Ref. [10] focused on investigating different asymmetric bistable systems that were driven by multiplicative and additive Gaussian white noise. In Ref. [11], the authors presented a time-delayed bistable system and analyzed the phenomenon of SR using statistical complexity measure and normalized Shannon entropy. Although Gaussian noise is widely used and easy to analyze, the probability density distribution of noise in real applications is often more complex. To apply SR in practical engineering, scholars have turned to research on nonlinear systems driven by non-Gaussian noise [12–18]. Fuentes et al. [13] observed the SR phenomenon in bistable systems driven by non-Gaussian noise and found that the resonance effect was enhanced when the noise deviated from the Gaussian distribution. Jin and Li [14] proposed a piecewise bistable system induced by correlated multiplicative and additive color noise and derived the expression of output signal-to-noise ratio (SNR) using two-state theory. They also investigated the effects of color noise on SNR. Guo et al. [15] studied and analyzed SR in piecewise bistable systems under multiplicative non-Gaussian noise and additive Gaussian white noise. The results showed that the effects of non-Gaussian noise and Gaussian white noise on SNR are different. In Ref. [16], a coupled bistable SR system driven by levy noise was proposed, and the effects of system parameters on the mean signal-to-noise gain were studied. Additionally, scholars have researched SR driven by non-Gaussian noise in neural networks. In Ref. [17], a simplified one-dimensional F-N neural network driven by correlated multiplicative non-Gaussian noise and additive Gaussian white noise was studied. In Ref. [18], SR phenomenon in time-delayed F-N neural networks driven by non-Gaussian noise was studied,

*Corresponding author, E-mail: 1510855227@qq.com

and the effects of time delay and non-Gaussian noise strength on SNR were discussed.

Recent studies have shown that the dynamics of tri-stable systems are more complex and exhibit better performance than bistable systems, leading to extensive research on tri-stable systems [19–23]. In Ref. [19], a standard underdamped tri-stable SR system was proposed through parameter transformation based on the classical tri-stable system. In Ref. [20], a piecewise tri-stable SR system was proposed and applied in bearing fault detection. The SR phenomenon in a tri-stable system with time-delayed feedback was studied, and the effects of time delay strength and length on SNR were explored in Ref. [21]. However, these studies on tri-stable SR systems are all based on Gaussian white noise, and very few papers have investigated tri-stable SR systems driven by non-Gaussian noise, which exhibits properties more consistent with real noise. Additionally, the analysis of the resonance behavior of an asymmetric tri-stable system is more complex than that of a symmetric tri-stable SR system. Moreover, the derivation of the spectrum amplification becomes further complicated when the system is driven by multiplicative non-Gaussian noise and additive Gaussian white noise. Hence, based on the above discussions, this paper proposes an ATSSR system driven by correlated multiplicative non-Gaussian noise and additive Gaussian white noise.

The contents of this paper are organized as follows: In Sect. 1, the potential structure of ATSSR system is analyzed. In Sect. 2, the specific expressions of SPD, MFPT, and SA are derived under the limit of adiabatic approximation, and the effects of each parameter on them are analyzed. In Sect. 3, a periodic attenuated pulse signal and a harmonic vibration signal are constructed, and simulated fault signal detection experiments are performed using the ATSSR system. Finally, the conclusions and outlook are provided for future research in Sect. 4.

2. ATSSR system

2.1. System model

Driven by a periodic forcing and correlated multiplicative non-Gaussian noise and additive Gaussian white noise, ATSSR system can be described as the Langevin equation of Eq. (1):

$$\dot{x} = -\dot{U}(x) + A_0\cos(2\pi f_0 t) + x\varsigma(t) + \varepsilon(t) \tag{1}$$

where A_0 and f_0 are the amplitude and frequency of the external periodic forcing, respectively.

$U(x) = x^2(a - bx)(a + x) + cx^6$ is the asymmetric tri-stable potential function, and a, b, and c are positive real numbers. Since the symmetry of the potential function is not related to the parameter c, without loss of generality, c is fixed as $c = 0.2$ in Fig. 1. As can be shown, ATSSR system has three stable points s_1, s_2, and s_3, and two unstable points u_1 and u_2. For convenience, s_1, s_2, and s_3 are called the potential well on the left, middle, and right, respectively. It can be seen that the depth and width of the left and right potential wells become shallower and narrower, respectively, while the depth of the middle potential well increases as a increases. Nevertheless, the height of the middle barrier decreases as b increases.

In Eq. (1), $\varepsilon(t)$ is a Gaussian white noise with the statistical characteristic: $\langle\varepsilon(t)\rangle = 0$, $\langle\varepsilon(t)\varepsilon(t_1)\rangle = 2Q\delta(t - t_1)$. $\varsigma(t)$ can be generated by the following equation:

$$\frac{d\varsigma(t)}{dt} = -\frac{1}{\tau_1}\frac{d}{d\varsigma}V_q(\varsigma) + \frac{1}{\tau_1}\xi(t) \tag{2a}$$

$$V_q(\varsigma) = \frac{D}{\tau_1(q-1)}\ln\left(1 + \frac{\tau_1(q-1)}{D}\frac{\varsigma^2}{2}\right) \tag{2b}$$

The process $\varsigma(t)$ is consistent with the Ornstein–Uhlenbeck process when $q = 1$, while it is a non-Gaussian process when $q \neq 1$. And the first-order and second-order moments of $\varsigma(t)$ satisfy:

$$\langle\varsigma(t)\rangle = 0 \tag{3a}$$

$$\left\langle\varsigma^2(t)\right\rangle = \begin{cases} \frac{2D}{\tau_1(5-3q)}, & q \in \left(-\infty, \frac{5}{3}\right) \\ \infty, & q \in \left(\frac{5}{3}, 3\right) \end{cases} \tag{3b}$$

D and τ_1 are noise intensity and correlation time, respectively, and q represents the degree of deviation of $\varsigma(t)$ from the Gaussian distribution. $\xi(t)$ is a Gaussian white noise with mean value 0 and intensity D, and its correlation intensity and correlation time with $\varepsilon(t)$ are λ and τ_2, respectively, that is: $\langle\xi(t)\varepsilon(t_1)\rangle = \langle\xi(t_1)\varepsilon(t)\rangle = 2\lambda\frac{\sqrt{DQ}}{\tau_2}\delta(t - t_1)$.

According to Ref. [24], when $|q - 1| << 1$, i.e., $\varsigma(t)$ slightly deviates from the Gaussian distribution, it can be obtained:

$$\begin{aligned}\frac{1}{\tau_1}\frac{d}{d\varsigma}V_q(\varsigma) &= \frac{\varsigma}{\tau_1}\left[1 + \frac{\tau_1}{D}(q-1)\frac{\varsigma^2}{2}\right]^{-1} \\ &\approx \frac{\varsigma}{\tau_1}\left[1 + \frac{\tau_1}{D}(q-1)\frac{\langle\varsigma^2\rangle}{2}\right]^{-1}\end{aligned} \tag{4}$$

for $q < \frac{5}{3}$, $\left\langle\varsigma^2(t)\right\rangle = \frac{2D}{\tau_1(5-3q)}$. Therefore, Eq. (4) can be simplified as follows:

$$\frac{1}{\tau_1}\frac{d}{d\varsigma}V_q(\varsigma) = \frac{1}{\tau_1}\frac{5-3q}{2(2-q)}\varsigma(t) = \frac{1}{\tau_{\text{eff}}}\varsigma(t) \tag{5}$$

where τ_{eff} is the effective correlation time and $\tau_{\text{eff}} = \frac{2(2-q)}{5-3q}\tau_1$.

Taking Eq. (4) into Eq. (2a), it is obtained:

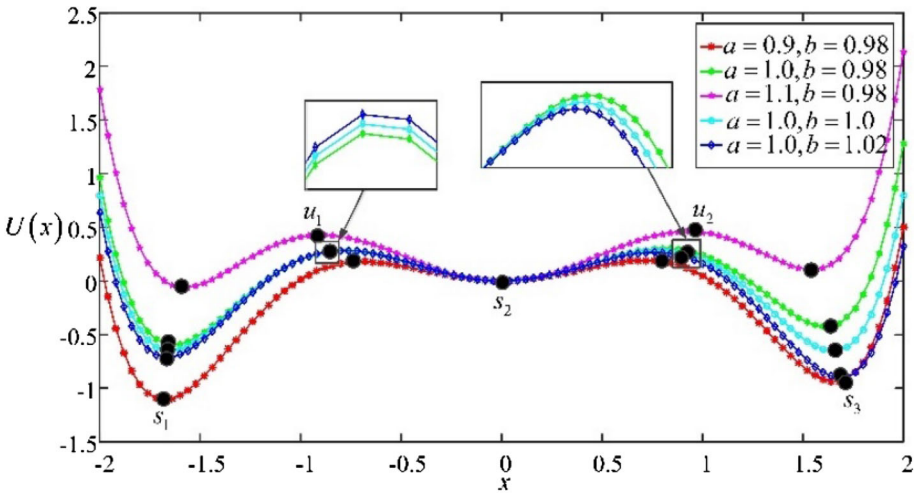

Fig. 1 Potential structure

$$\frac{d\varsigma(t)}{dt} = -\frac{1}{\tau_{\text{eff}}}\varsigma(t) + \frac{1}{\tau_{\text{eff}}}\xi_1(t) \tag{6}$$

where $\xi_1(t)$ is a Gaussian white noise, which satisfies: $\langle \xi_1(t) \rangle = 0$, $\langle \xi_1(t)\xi_1(t_1) \rangle = 2D_{\text{eff}}\delta(t - t_1)$. D_{eff} is the effective noise intensity and $D_{\text{eff}} = \left[\frac{2(2-q)}{5-3q}\right]^2 D$.

$\xi_1(t)$ and $\varepsilon(t)$ are cross-correlated noise with correlation strength λ and correlation time τ_2:

$$\langle \xi_1(t)\varepsilon(t_1) \rangle = \langle \xi_1(t_1)\varepsilon(t) \rangle = 2\lambda \frac{\sqrt{D_{\text{eff}}Q}}{\tau_2}\delta(t - t_1) \tag{7}$$

Applying the unified color noise approximation, the Markov process of Eq. (1) is:

$$\dot{x} = \frac{1}{A_h(x, \tau_1)}[h(x, t) + x\xi_1(t) + \varepsilon(t)] \tag{8}$$

where $h(x, t) = -\dot{U}(x) + A_0 \cos(2\pi f_0 t)$, $A_h(x, \tau_{\text{eff}}) = 1 - \tau_{\text{eff}}\left[\frac{d}{dx}h(x, t) - \frac{1}{x}h(x, t)\right]$, and $A_h(x, \tau_{\text{eff}}) > 0$.

Equation (8) can be rewritten as the differential form of Eq. (9):

$$\dot{x} = \alpha(x) + \beta(x)\Gamma(t) \tag{9}$$

where $\alpha(x) = \frac{h(x,t)}{A_h(x,\tau_1)}$, $\beta(x) = \frac{\left(D_{\text{eff}}x^2 + 2\lambda\sqrt{D_{\text{eff}}Q}x/(1+2\tau_2) + Q\right)^{1/2}}{A_h(x,\tau_1)}$, and the statistical properties of $\Gamma(x)$ are: $\langle \Gamma(t) \rangle = 0$, $\langle \Gamma(t)\Gamma(t - t_1) \rangle = 2\delta(t - t_1)$.

2.2. Steady-state probability density of ATSSR system

The Fokker–Planck equation of Eq. (10) can be approximated as follows:

$$\frac{\partial \rho(x, t)}{\partial t} = -\frac{\partial}{\partial x}[\alpha(x, t) + \beta(x)\beta'(x)]\rho(x, t) + \frac{\partial^2}{\partial x^2}\beta^2(x)\rho(x, t) \tag{10}$$

The steady-state probability density (SPD) function is:

$$\rho_{\text{st}}(x) = \frac{N}{\beta(x)}\exp\left[-\frac{\tilde{U}(x, t)}{D_{\text{eff}}}\right] \tag{11}$$

where $N = \left[\int \frac{\exp\left[-\tilde{U}(x,t)/D_{\text{eff}}\right]}{\beta(x)}\right]^{-1}$ is the normalization constant, and $\tilde{U}(x, t)$ is the generalized potential function whose expression is:

$$\tilde{U}(x, t) = D_{\text{eff}} \int \frac{U'(x) - A_0 \cos(2\pi f_0 t)}{x^2 + 2\lambda\sqrt{D_{\text{eff}}Q}x/(1 + 2\tau_2) + Q} A_h(x, \tau_1)dx \tag{12}$$

By neglecting the second-order term of A_0 in $\tilde{U}(x, t)$, we can obtain:

$$\tilde{U}(x, t) = U_0(x) - A_0 g(x)\cos(2\pi f_0 t) + o\left(A_0^2\right) \tag{13}$$

Setting $a = 1.5$, $c = 0.1$, $\tau_1 = 0.1$, $\tau_2 = 0.1$, Fig. 2

$$U_0(x) = D_{\text{eff}} \int \frac{\left[6cx^5 - 4bx^3 + 3a(1 - b)x^2 + 2ax\right]\left\{1 - \tau_{\text{eff}}\left[-24cx^4 + 8bx^2 - 3a(1 - b)x\right]\right\}}{x^2 + 2\lambda(1 + 2\tau_2)^{-1}\sqrt{D_{\text{eff}}Q}x + Q}dx \tag{14}$$

$$g(x) = D_{\text{eff}} \int \frac{\left\{1 - \tau_{\text{eff}}\left[-24cx^4 + 8bx^2 - 3a(1 - b)x\right]\right\} - \tau_{\text{eff}}\left[6cx^4 - 4bx^2 + 3a(1 - b)x + 2a\right]}{x^2 + 2\lambda(1 + 2\tau_2)^{-1}\sqrt{D_{\text{eff}}Q}x + Q}dx \tag{15}$$

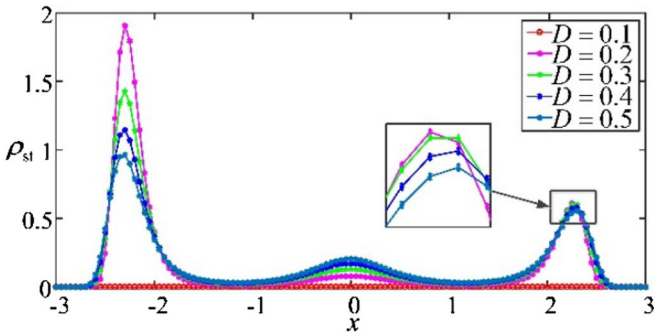

(a) Steady-state probability density as a function of D (b=0.98, $\lambda = 0.1$, q=1, Q=0.5)

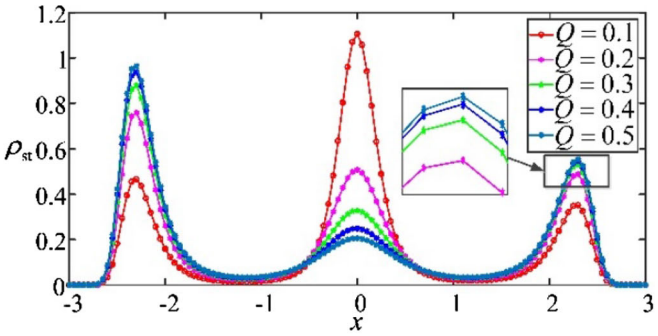

(b) Steady-state probability density as a function of Q (b=0.98, $\lambda = 0.1$, q=1, D=0.5)

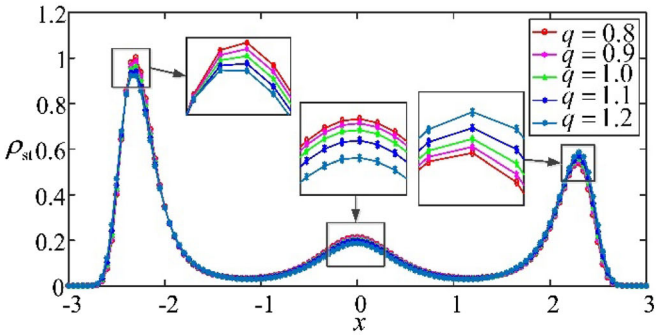

(c) Steady-state probability density as a function of q (b=0.98, $\lambda = 0.1$, D=0.5, Q=0.5)

Fig. 2 Curves of steady-state probability density under different parameters. (**a**) Steady-state probability density as a function of D (b = 0.98, $\lambda = 0.1$, q = 1, Q = 0.5). (**b**) Steady-state probability density as a function of Q (b = 0.98, $\lambda = 0.1$, q = 1, D = 0.5). (**c**) Steady-state probability density as a function of q (b = 0.98, $\lambda = 0.1$, D = 0.5, Q = 0.5). (**d**) Steady-state probability density as a function of λ (b = 0.98, q = 1, D = 0.5, Q = 0.5). (**e**) Steady-state probability density as a function of b ($\lambda = 0.1$, q = 1, D = 0.5, Q = 0.5)

shows the effects of certain parameters of the two noises and the asymmetric intensity on the particle motion states. In Fig. 2(a), SPD on the left and right potential wells decreases, while SPD on the middle potential well increases when D increases, which indicates that particles are more prone to transit from the outermost potential wells to the middle potential well. In Fig. 2(b), the effect of Q on SPD is opposite to D, the probability of particles transition from the middle to the outermost potential wells increases as Q increases. In Fig. 2(c), SPD on the left and the middle potential well decreases, while SPD on the right potential well increases when q increases. In Fig. 2(d), with the increase in λ, SPD increases on the left potential well and decreases on both right and middle potential wells. In Fig. 2(e), SPD on the right potential well is greater than the left one when $b > 1$, since the depth of the right potential well is larger and particles are less likely to transit. In addition, SPD rises on right potential well and falls on middle and left potential wells when $b > 1$, and vice versa when $b < 1$.

Fig. 2 continued

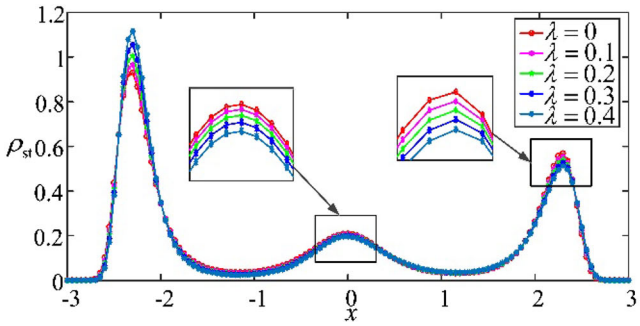

(d) Steady-state probability density as a function of λ (b=0.98, q=1, D=0.5, Q=0.5)

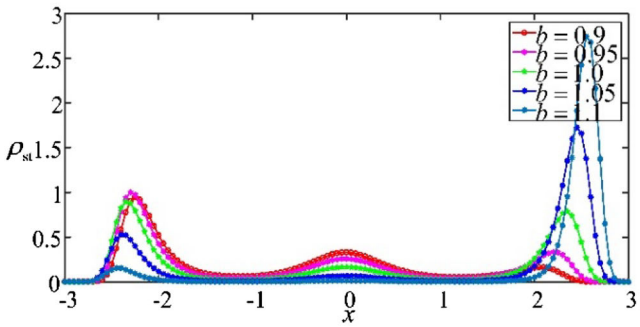

(e) Steady-state probability density as a function of b ($\lambda = 0.1$, q=1, D=0.5, Q=0.5)

2.3. Mean First-Pass Time of ATSSR system

In this section, the escape of particles through Mean First-Pass Time (MFPT) is analyzed. By defining $T_{s_1 \to s_2}$ as the MFPT of the particles from s_1 to s_2, according to the definition of MFPT, it can be obtained that:

$$T_{s_1 \to s_2} = \int_{s_1}^{s_2} \frac{dx}{\sqrt{\beta(x)}\rho_{\mathrm{st}}(x)} \int_{-\infty}^{x} dy \rho_{\mathrm{st}}(y) = \frac{2\pi}{\sqrt{U''(s_1)U''(u_1)}} \exp\left[\frac{\tilde{U}(u_1,t) - \tilde{U}(s_1,t)}{D_{\mathrm{eff}}}\right] \quad (16)$$

Similarly:

$$T_{s_2 \to s_3} = \int_{s_2}^{s_3} \frac{dx}{\sqrt{\beta(x)}\rho_{st}(x)} \int_{-\infty}^{x} dy \rho_{st}(y) = \frac{2\pi}{\sqrt{U''(s_2)U''(u_2)}} \exp\left[\frac{\tilde{U}(u_2,t) - \tilde{U}(s_2,t)}{D_{\mathrm{eff}}}\right] \quad (17)$$

Figure 3 demonstrates the variation of $\ln(T_{s_1 \to s_2})$ with D which shows a decreasing trend as D increases, indicating that the time for the particles to transit from s_1 to s_2 decreases. This is because as the multiplicative noise intensity increases, the more energy is available to facilitate particles transit and the shorter the time required for the transition. In Fig. 3(a), $\ln(T_{s_1 \to s_2})$ decreases when q increases, which indicates that less time is needed for particles to transit from s_1 to s_2 as the deviation of $\varsigma(t)$ from the Gaussian distribution increases. In Fig. 3(b), $\ln(T_{s_1 \to s_2})$ is smaller when the two noises are not correlated and the time for particles to transit from s_1 to s_2 increases as λ increases. The power of two uncorrelated noises can be superimposed, while the power of the correlated noise cannot be superimposed; thus, the particles can get more energy to transit when additive noise and multiplicative noise are correlated. However, as λ increases, the correlated intensity of the two noises increases, which leads to an increase in the transit time.

Similarly, Fig. 4 shows the variation of $\ln(T_{s_1 \to s_2})$ with Q, which can be seen that $\ln(T_{s_1 \to s_2})$ decreases as Q increases. Since the increase in additive noise intensity also provides more energy for the particles to transit and facilitates the transition. But the effects of q and λ on $\ln(T_{s_1 \to s_2})$ are different, $\ln(T_{s_1 \to s_2})$ decreases when q increases, while $\ln(T_{s_1 \to s_2})$ increases as λ increases. Figure 5 shows the effects of D and Q on $\ln(T_{s_1 \to s_2})$ for both symmetric and asymmetric potential functions, which can be seen that $\ln(T_{s_1 \to s_2})$ decreases with increasing D or Q. But when the potential function is symmetrically distributed, the particles take more time to transit from s_1 to s_2. This is because the potential well on the left side is

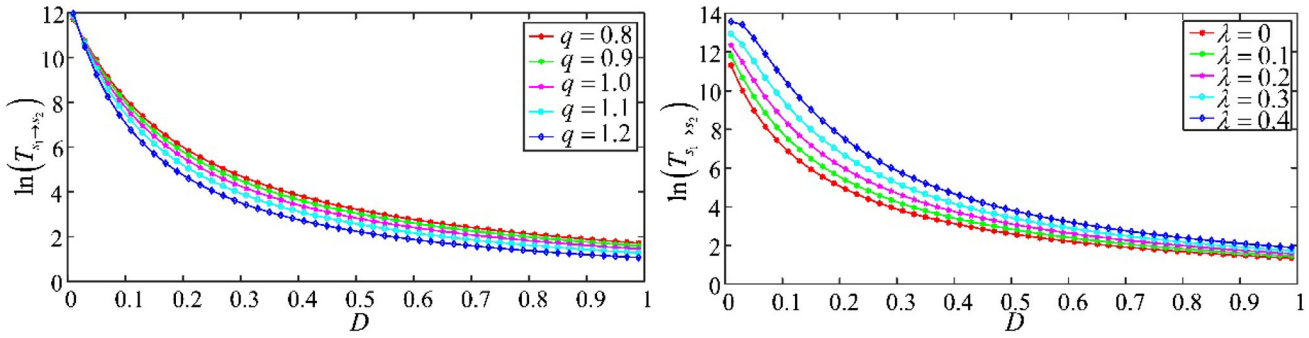

(a) $\lambda = 0.1$ (b) q=1

Fig. 3 Mean First-Pass Time of particles from s_1 to s_2 as a function of D (a = 1, b = 0.8, c = 0.1, $\tau_1 = 0.1$, $\tau_2 = 0.1$, Q = 0.5)

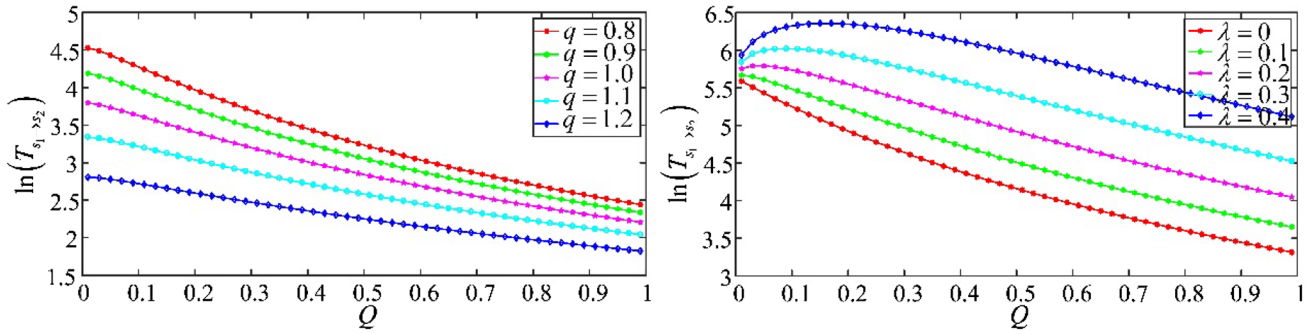

(a) $\lambda = 0.1$ (b) q=1

Fig. 4 Mean First-Pass Time of particles from s_1 to s_2 as a function of Q (a = 1, b = 0.8, c = 0.1, $\tau_1 = 0.1$, $\tau_2 = 0.1$, D = 0.5)

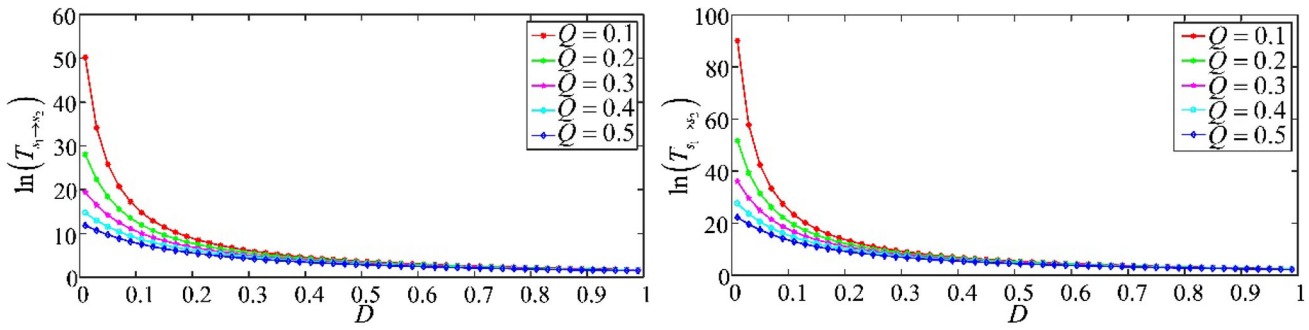

(a) b=0.8 (c) b=1

Fig. 5 Mean First-Pass Time of particles from s_1 to s_2 as a function of D and Q under different b (a = 1, c = 0.1, $\tau_1 = 0.1$, $\tau_2 = 0.1$, $\lambda = 0.1$, q = 1)

deeper, and it is more difficult for particles to transit from the left side potential well to the middle potential well when b = 1, which is consistent with the previous theoretical results.

Figures 6 and 7 describe the variation of $\ln(T_{s_2 \to s_3})$ with D and Q, respectively. $\ln(T_{s_2 \to s_3})$ decreases with the increases in D or Q, indicating that when the external energy increases, less time is needed for particles to transit. Whether $\ln(T_{s_2 \to s_3})$ as a function of D or Q, $\ln(T_{s_2 \to s_3})$ decreases as q or λ increases.

Figure 8 indicates the variation of $\ln(T_{s_2 \to s_3})$ with D and Q under different b. Similarly, $\ln(T_{s_2 \to s_3})$ decreases in both cases as D or Q increases. However, different from Fig. 5, the transit time of the particles from s_2 to s_3 is shorter

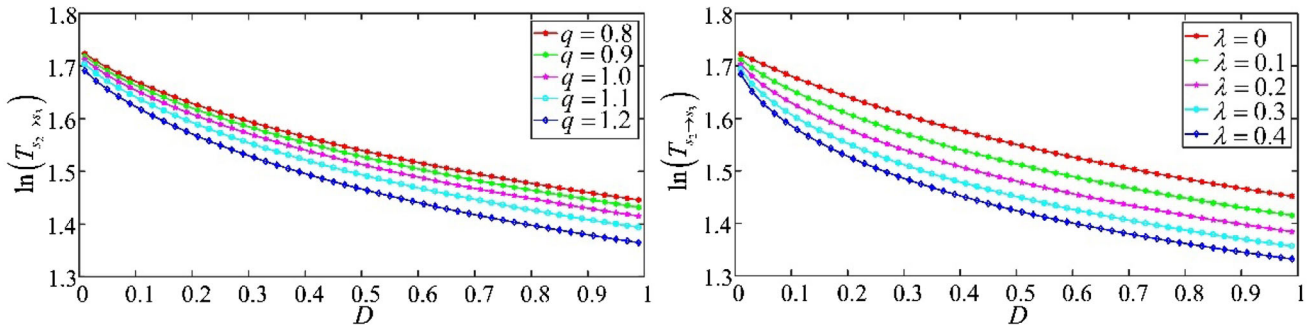

(a) $\lambda = 0.1$ (b) q=1

Fig. 6 Mean First-Pass Time of particles from s_2 to s_3 as a function of D (a = 1, b = 0.8, c = 0.1, $\tau_1 = 0.1$, $\tau_2 = 0.1$, Q = 0.5)

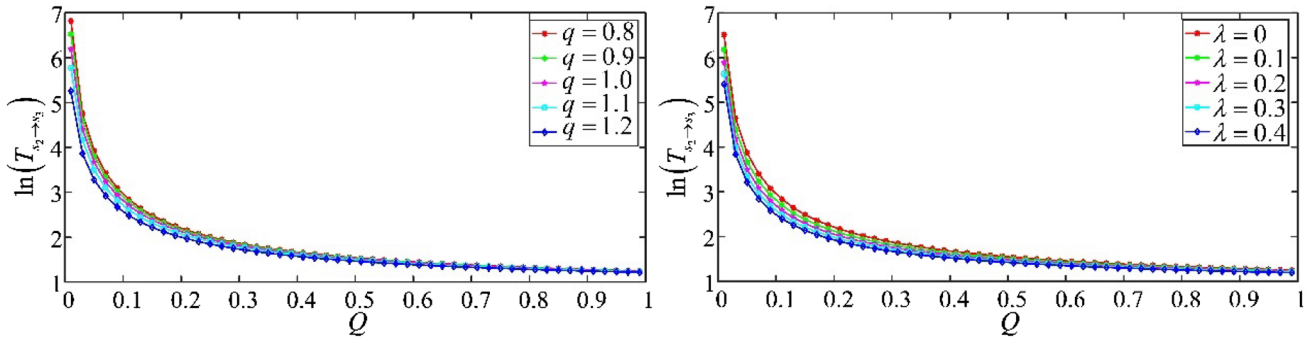

(a) $\lambda = 0.1$ (b) q=1

Fig. 7 Mean First-Pass Time of particles from s_2 to s_3 as a function of Q (a = 1, b = 0.8, c = 0.1, $\tau_1 = 0.1$, $\tau_2 = 0.1$, D = 0.5)

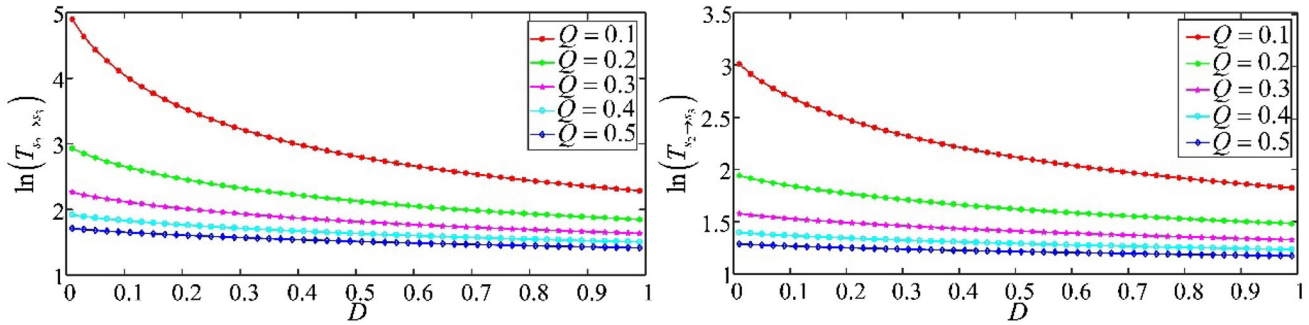

(a) b=0.8 (b) b=1

Fig. 8 Mean First-Pass Time of particles from s_2 to s_3 as a function of D and Q under different b (a = 1, c = 0.1, $\tau_1 = 0.1$, $\tau_2 = 0.1$, $\lambda = 0.1$, q = 1)

because the depth of the middle potential well is significantly less than the depth of the potential wells on either side when the potential function is symmetric.

2.4. Spectrum amplification

To further analyze the SR behavior of particles, this section examines the spectral amplification factor of ATSSR system. Assume that $p_i (i = 1, 2, 3)$ is the probability of a Brownian particle at the steady-state point $s_i (i = 1, 2, 3)$ and $\sum p_i = 1$. The master equation for p_i can be obtained as follows:

$$\frac{dp_i}{dt} = \sum_{j=1}^{3} R_{i,j} p_j \tag{18}$$

where R is the transition matrix, and its specific expression is shown in Appendix A.

The probability flow equation of Eq. (18) can be decomposed as follows:

$$p_i = p_i^{(0)} + A_0 \Delta p_i \tag{19}$$

Substituting Eq. (19) into Eq. (18), it is obtained as follows:

$$\frac{d\Delta p_i}{dt} = \sum_{j=1}^{3} R_{i,j}^{(0)} \Delta p_j + \phi_i \cos(2\pi f_0 t) \tag{20}$$

Among them, $R^{(0)}$ represents the undisturbed transition matrix, and ϕ can be expressed as follows:

$$\phi = \frac{1}{D_{\text{eff}}} \begin{pmatrix} -r_{1,2}^{(0)} \Delta g_{1,2} p_1^{(0)} + r_{2,1}^{(0)} \Delta g_{2,1} p_2^{(0)} \\ r_{1,2}^{(0)} \Delta g_{1,2} p_1^{(0)} - \left(r_{2,1}^{(0)} \Delta g_{2,1} + r_{2,3}^{(0)} \Delta g_{2,3} \right) p_2^{(0)} + r_{3,2}^{(0)} \Delta g_{3,2} p_3^{(0)} \\ r_{2,3}^{(0)} \Delta g_{2,3} p_2^{(0)} - r_{3,2}^{(0)} \Delta g_{3,2} p_3^{(0)} \end{pmatrix} \tag{21}$$

Under the limit of long time, the simplified Eq. (21) is:

$$\Delta p_i = \lambda_i \sin(2\pi f_0 t) + \sigma_i \cos(2\pi f_0 t) \tag{22}$$

Combining Eqs. (20) and (22), the specific expressions of λ_i and σ_i are:

$$\begin{aligned} \lambda_i &= \sum_{j=1}^{3} 2\pi f_0 \left[\mu_j^2 + (2\pi f_0)^2 \right]^{-1} a_j v_{j,i}, \\ \sigma_i &= \sum_{j=1}^{3} \mu_j \left[\mu_j^2 + (2\pi f_0)^2 \right]^{-1} a_j v_{j,i} \end{aligned} \tag{23}$$

where μ_j and v_j are the eigenvalues and corresponding eigenvectors of $R^{(0)}$, respectively, and a_j is the expansion coefficients of ϕ, satisfying $\phi = \sum_{j=1}^{3} a_j v_j$.

The mean time response of the system by a periodic signal is:

$$\begin{aligned} \langle x(t) | x_0, t_0 \rangle &= \int x P(x, t | x_0, t_0) dx \\ &= \int x \sum_{i=1}^{3} p_i(t) \delta(x - s_i) dx \end{aligned} \tag{24}$$

When $t_0 \to -\infty$, Eq. (24) can be expressed as follows:

$$\langle x(t) \rangle_{\text{as}} = A \sin(2\pi f_0 t + \psi) \tag{25}$$

where A and ψ are the amplitude and phase of the asymptotic average response, respectively:

$$A = A_0 \sqrt{\left[\sqrt{(s_1 A_1)^2 + 2 s_1 s_2 A_1 A_2 \cos(\Gamma_1) + (s_2 A_2)^2} + s_3 A_3 \cos(\Gamma_2) \right]^2 + [s_3 A_3 \sin(\Gamma_2)]^2} \tag{26}$$

With $A_i = \sqrt{\lambda_i^2 + \sigma_i^2}$, $\psi_i = \arctan(\sigma_i / \lambda_i)$, $\Gamma_1 = \psi_2 - \psi_1$, $\Gamma_2 = \psi_3 - \psi_1 - \Lambda_1$, $\Lambda_1 = \arctan\{s_2 A_2 \sin(\Gamma_1) / [s_1 A_1 + s_2 A_2 \cos(\Gamma_1)]\}$.

Therefore, the SA of ATSSR system is:

$$\begin{aligned} \eta &= \frac{A^2}{A_0^2} \\ &= \sum_{i=1}^{3} (s_i A_i)^2 + 2 s_1 s_2 A_1 A_2 \cos(\Gamma_1) \\ &\quad + 2 s_3 A_3 \cos(\Gamma_2) \sqrt{\sum_{i=1}^{2} (s_i A_i)^2 + 2 s_1 s_2 A_1 A_2 \cos(\Gamma_1)} \end{aligned} \tag{27}$$

Since $s_2 = 0$, η is simplified as follows:

$$\eta = (s_1 A_1)^2 + (s_3 A_3)^2 + 2 |s_1 A_1| s_3 A_3 \cos(\Gamma_2) \tag{28}$$

Setting $a = 1$, $c = 0.1$, $\tau_1 = 0.1$, $\tau_2 = 0.1$, Fig. 9 and Fig. 10 describe the variation of η with D, where η first increases and then decreases as D increases, indicating that the system occurs in stochastic resonance and that D corresponding to the peak is the noise energy required for the system to achieve optimal synergy. In Fig. 9, the peak of η corresponds to a smaller D as q increases. The difference is that when the potential function is symmetric, η is greater, but the system requires more energy for the occurrence of SR. In Fig. 10, η as a function of D varies with λ changes under different b. When $b = 0.8$, the peak of η increases and the corresponding D decreases with the increase in λ, while the peak value of η decreases and the corresponding D increases when $b = 1$.

Figures 11 and 12 show the variation of η with Q. Similarly, as Q increases, there is a single peak, indicating the occurrence of SR. In Fig. 11, the peak of η increases as q increases and its position shifts to the right, but the peak is higher when $b = 1$. In Fig. 12, the peak of η decreases with increasing λ, at the same time, the peak is higher for $b = 1$.

Figure 13 discusses the influence of D and Q on η. In Fig. 13(a), when the potential structure is asymmetric, η as a function of D, the peak value increases and the corresponding position of the peak shifts to the left with the increase in Q. But when $Q > 0.3$, SR phenomenon disappears. In Fig. 13(b), when the potential structure is sym-

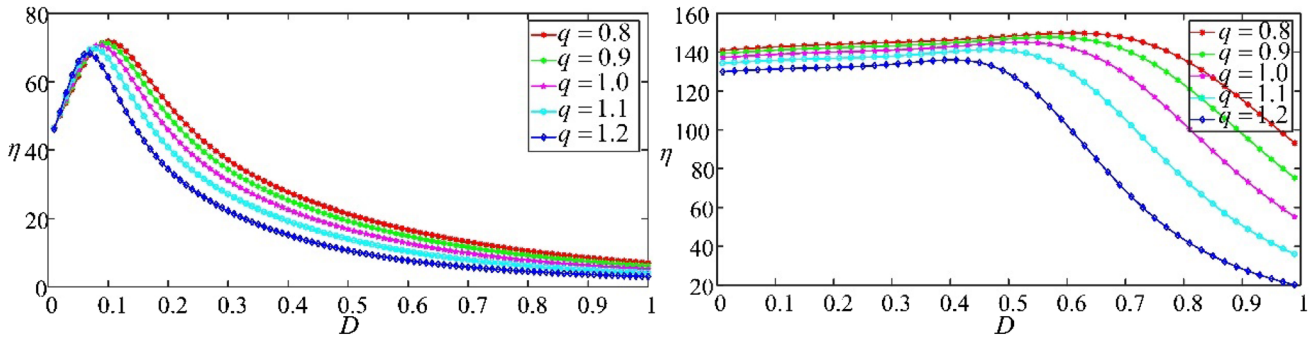

(a) b=0.8 (b) b=1

Fig. 9 Spectrum amplification (η) as a function of D and q under different b ($\lambda = 0.1$, $Q = 0.2$)

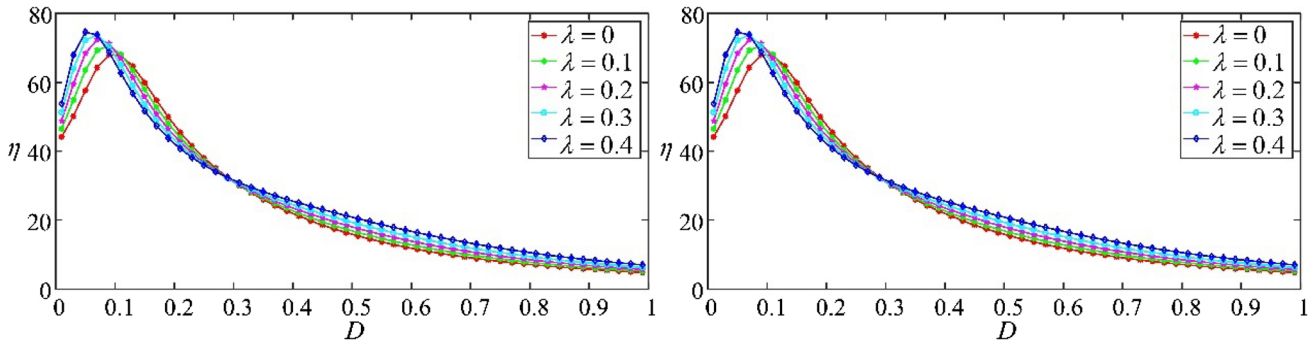

(a) b=0.8 (b) b=1

Fig. 10 Spectrum amplification (η) as a function of D and λ under different b ($q = 1$, $Q = 0.2$)

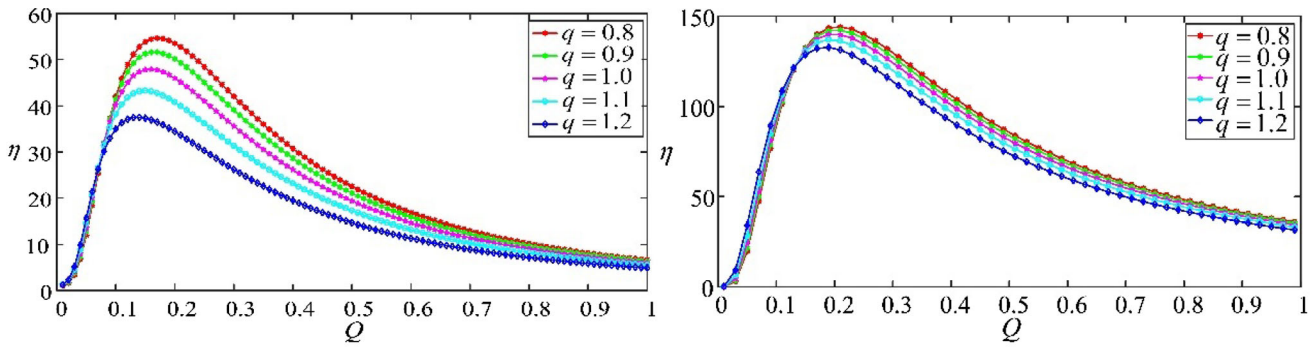

(a) b=0.8 (b) b=1

Fig. 11 Spectrum amplification (η) as a function of Q and q under different b ($\lambda = 0.1$, $D = 0.2$)

metrical, the peak value decreases and the corresponding D decreases with the increase in Q. And η always decreases with the increase in D when $Q > 0.2$, then no sign of the SR phenomenon can be observed.

3. Numerical simulations

To verify the feasibility of the proposed ATSSR system in weak signal detection, a periodic attenuated pulse signal and a harmonic vibration signal are constructed for simulation experiments.

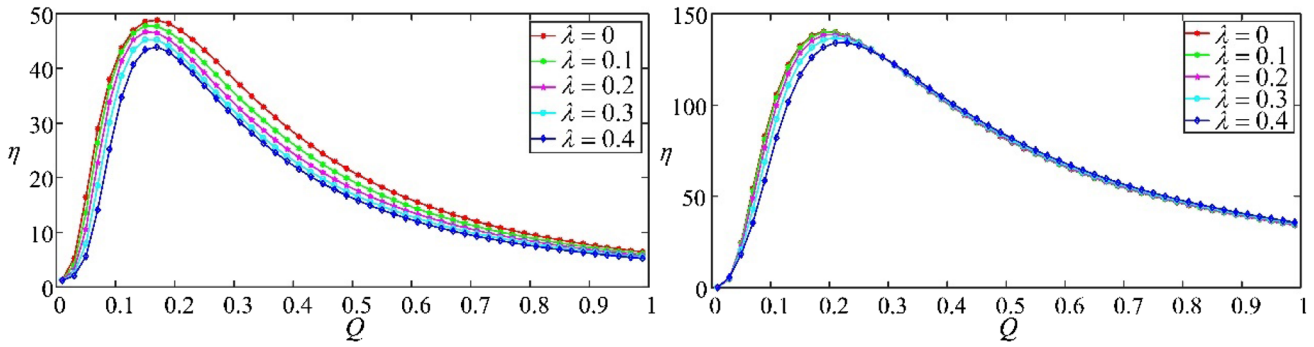

(a) b=0.8 (b) b=1

Fig. 12 Spectrum amplification (η) as a function of Q and λ under different b (q = 1, D = 0.2)

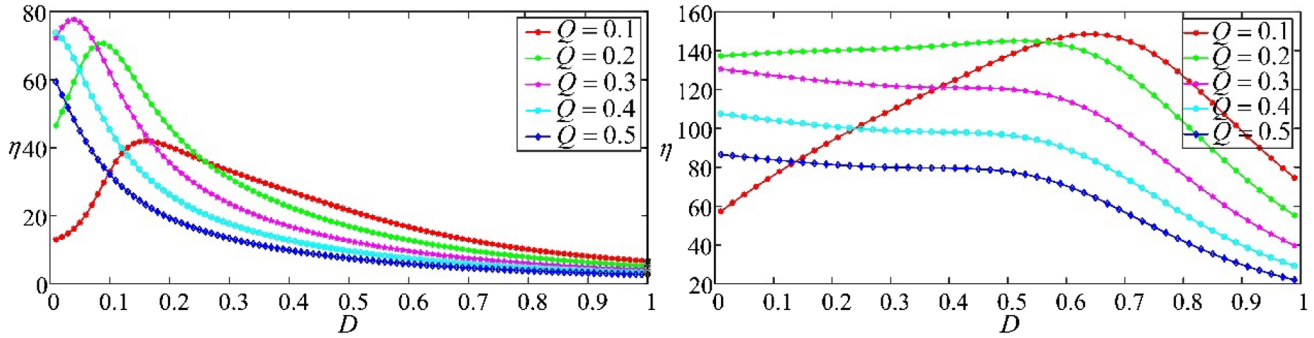

(a) b=0.8 (b) b=1

Fig. 13 Spectrum amplification (η) as a function of D and Q under different b ($\lambda = 0.1$, q = 1)

3.1. A periodically attenuated pulse signal detection

Bearings are commonly found in a variety of machinery and their fault signals can take many forms, some of which are in the form of shocks in order to effectively detect faulty bearings at an early stage and reduce losses. Therefore, periodically attenuated pulse signal is constructed to simulate the signal collected when an actual bearing fault occurs, and the ATSSR system is used for bearing fault signal detection to verify the practicality of the system.

$$s(t) = A\exp[-100(t - \lfloor t/T \rfloor/T)] \times \sin[100\pi(t - \lfloor t/T \rfloor/T)] \quad (32)$$

where sampling frequency $f_s = 2000$Hz, sampling points $N = 2000$, amplitude $A = 0.2$, period $T = 0.2$, and characteristic signal frequency $f = 1/T = 5$Hz. Figure 14(a) shows the time–frequency spectrum diagram of the original periodically attenuated pulse signal. Figure 14(b) shows the time–frequency diagram of the signal after adding Gaussian white noise with an intensity of 1.5. It shows that the signal is submerged in noise, and the fault characteristic signal frequency cannot be observed in the spectrogram under the background of strong noise. Since the characteristic signal frequency does not meet the requirement of small parameter, the secondary sampling is performed first and sampling frequency $f_{sr} = 5$Hz, and then, the fault signal is processed through ATSSR system. Figure 14(c) shows the time–frequency diagram of the output signal. A large amount of noise in the time-domain signal is filtered out, and the amplitude of the signal is amplified by nearly 5 times. In the frequency domain, a peak occurs at f = 4.998 Hz, with a difference of 15.9 from the subpeak. In addition, the peak at the characteristic frequency is more prominent than the surrounding noise components, which proves the feasibility of the system in signal detection.

3.2. A harmonic vibration signal detection

Rotating machines are widely used in systems such as generators, transportation, and medical equipment. It is a prerequisite to ensure their operational safety for reducing losses and avoiding personal injuries; thus, early fault

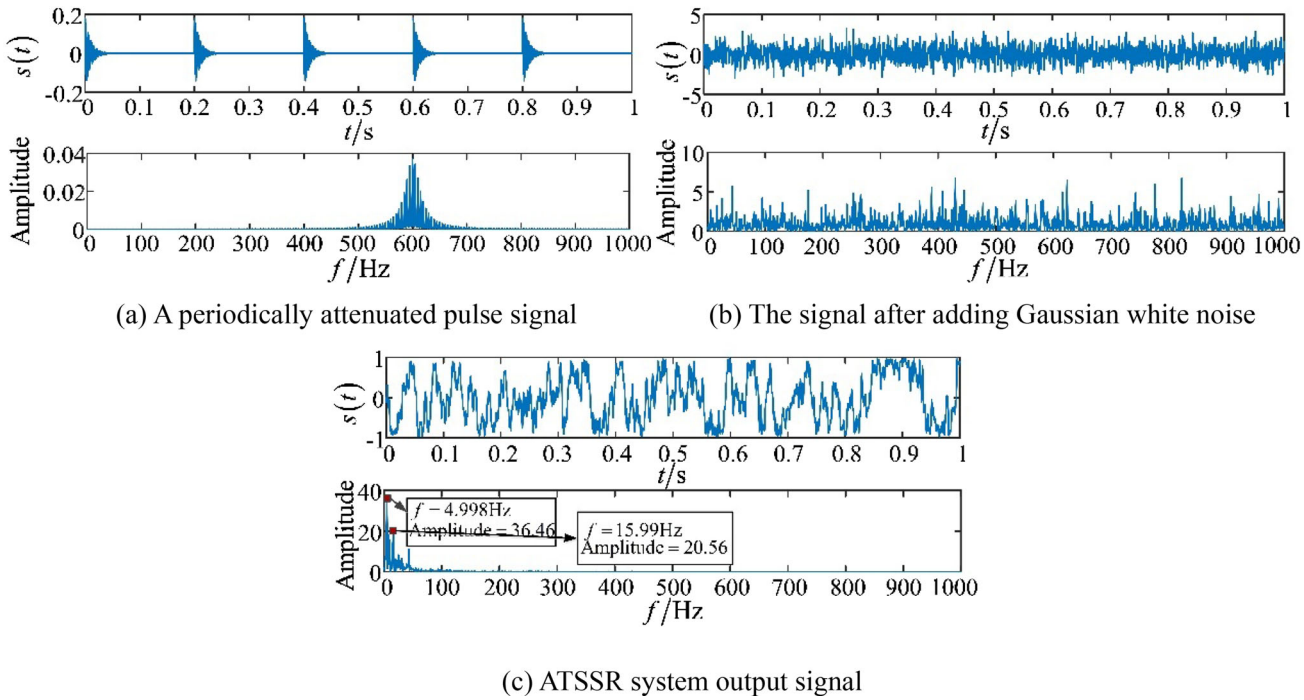

(a) A periodically attenuated pulse signal (b) The signal after adding Gaussian white noise

(c) ATSSR system output signal

Fig. 14 Periodically attenuated pulse signal detection based on ATSSR system. (**a**) A periodically attenuated pulse signal. (**b**) The signal after adding Gaussian white noise. (**c**) ATSSR system output signal

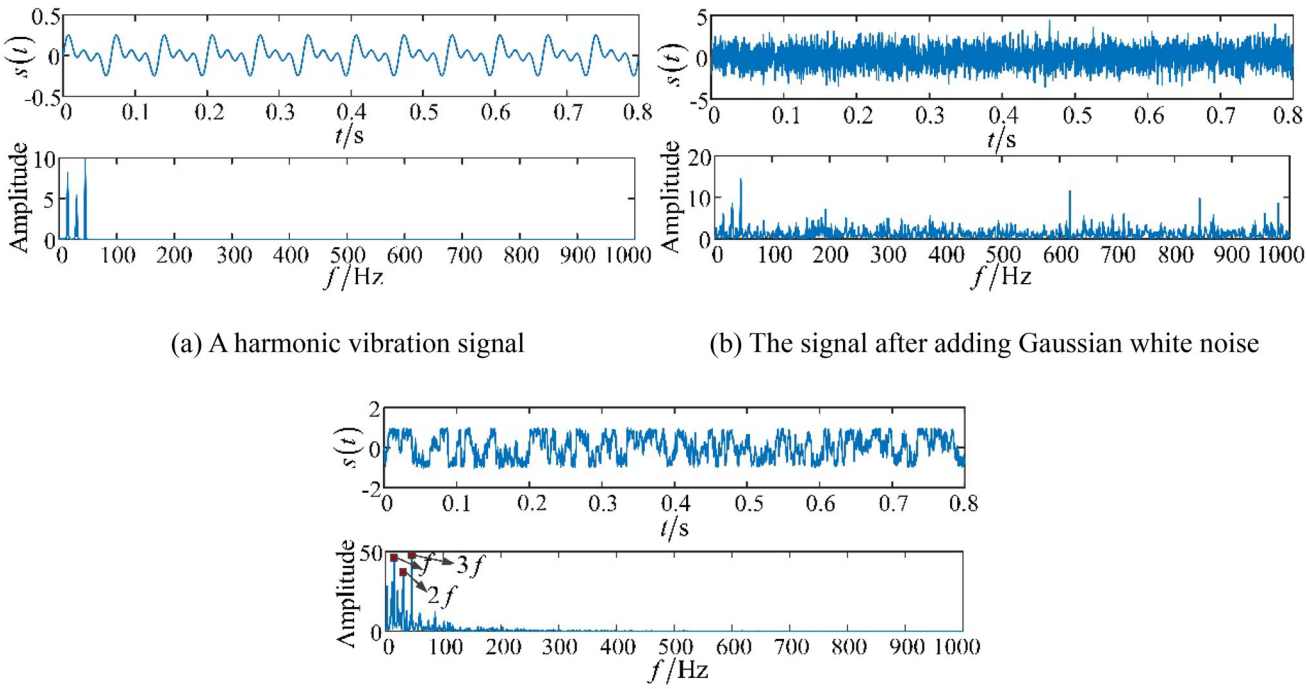

(a) A harmonic vibration signal (b) The signal after adding Gaussian white noise

(c) ATSSR system output signal

Fig. 15 Harmonic vibration signal detection based on ATSSR system. (**a**) A harmonic vibration signal. (**b**) The signal after adding Gaussian white noise. (**c**) ATSSR system output signal

prediction of rotating machines is very important. Generally, the operating status of the machine can be observed through the generated harmonic vibration signals of the rotating machinery system. The harmonic vibration signals

are mostly multi-frequency signals, so a vibration signal with three frequencies is constructed to verify its practicality:

$$s(t) = 0.1\sin(2\pi ft) + 0.1\sin(2\pi \times 2ft) + 0.1\sin(2\pi \times 3ft) \tag{33}$$

where the fundamental frequency $f = 15$ Hz, sampling frequency $f_s = 5000$ Hz, and sampling points $N = 4096$. Figure 15(a) shows the time domain and frequency spectrum of the original multi-frequency harmonic vibration signal. After adding Gaussian white noise with an intensity of 1.2, the time–frequency diagram of the signal is shown in Fig. 15(b). The signal is submerged in strong noise in the time domain and the frequency domain, and the periodicity and characteristic frequency of the signal cannot be observed. Since the three harmonic frequencies do not meet the small parameters, similarly, the secondary sampling is performed first and sampling frequency $f_{sr} = 5$ Hz, and then, the fault signal is processed through ATSSR system. Figure 15(c) shows the time–frequency diagram of output signal from ATSSR system. The time-domain signal is significantly less interfered by noise, and the signal waveform shows periodicity, and its amplitude is about twice that of the original signal. In addition, high-frequency noise is almost filtered out, and the amplitudes at the three harmonic frequencies are all higher than the surrounding noise components. The results indicate that the system can detect the characteristic frequency of the harmonic vibration fault signal.

4. Conclusions

In this paper, an asymmetric tri-stable potential function is proposed and its resonant behaviors driven by the periodic forces, and the correlated multiplicative non-Gaussian noise and additive Gaussian white noise are investigated. Firstly, the effects of D, Q, q, λ, and b on SPD and MFPT are analyzed. The main conclusions are as follows: (i) The effects of D and Q on SPD are opposite. (ii) Whether increasing D or Q, MFPT for particles to transit between wells is reduced. Then, the effects of D and Q on SA are analyzed for different q, λ, and b. The results show that η has single peak with the increasing in D or Q, indicating that parameter-induced SR appears. Besides, the asymmetric intensity has a significant effect on η. Finally, a periodic attenuated pulse signal and a harmonic vibration signal are constructed, and ATSSR system is used for simulated fault signal detection experiments. The experimental results exhibit good performances and prove the feasibility of ATSSR system in fault signal detection.

In this paper, we have only considered two typical correlation noises for fault detection analysis. However, practical applications involve various types of noise. Therefore, in further research, we plan to analyze the detection performance of this system under different combinations of noise sources. Moreover, to further improve the detection performance, we intend to search and construct new potential functions that can enhance the output signal-to-noise ratio.

Appendix A

R is the transition matrix, which is:

$$R = \begin{pmatrix} -r_{1,2} & r_{2,1} & 0 \\ r_{1,2} & -(r_{2,1} + r_{2,3}) & r_{3,2} \\ 0 & r_{2,3} & -r_{3,2} \end{pmatrix} \tag{A.1}$$

In the above formula, $r_{i,j}$ represents the transition probability of Brownian particles from s_i to s_j. The specific expression of $r_{i,j}$ is:

$$r_{m,m+1} = \frac{\sqrt{|U''(s_m)U''(u_m)|}}{2\pi}\exp\left[-\frac{\tilde{U}(u_m,t) - \tilde{U}(s_m,t)}{D_{\text{eff}}}\right], \quad m = 1, 2 \tag{A.2a}$$

$$r_{n,n-1} = \frac{\sqrt{|U''(s_n)U''(u_{n-1})|}}{2\pi}\exp\left[-\frac{\tilde{U}(u_{n-1},t) - \tilde{U}(s_n,t)}{D_{\text{eff}}}\right], \quad n = 2, 3 \tag{A.2b}$$

From Eq. (13), by expanding Eq. (A.2a) and Eq. (A.2b) to the first-order term of $\cos(2\pi f_0 t)$, it can be obtained:

$$r_{m,m+1} = r^{(0)}_{m,m+1} + A_0 D_{\text{eff}}^{-1} r^{(0)}_{m,m+1} \Delta g_{m,m+1}\cos(2\pi f_0 t) \tag{A.3a}$$

$$r_{n,n-1} = r^{(0)}_{n,n-1} + A_0 D_{\text{eff}}^{-1} r^{(0)}_{n,n-11} \Delta g_{n,n-1}\cos(2\pi f_0 t) \tag{A.3b}$$

With

$$r^{(0)}_{m,m+1} = \frac{\sqrt{|U''(s_m)U''(u_m)|}}{2\pi}\exp\left[-\frac{U_0(u_m) - U_0(s_m)}{D_{\text{eff}}}\right] \tag{A.4a}$$

$$r^{(0)}_{n,n-1} = \frac{\sqrt{|U''(s_n)U''(u_{n-1})|}}{2\pi}\exp\left[-\frac{U_0(u_{n-1}) - U_0(s_n)}{D_{\text{eff}}}\right] \tag{A.4b}$$

$$\Delta g_{m,m+1} = g(u_m, s_m), \Delta g_{n,n-1} = g(u_{n-1}, s_n) \tag{A.4c}$$

Acknowledgements This work is supported by the National Natural Science Foundation of China (No. 61771085), Research Project of Chongqing Educational Commission (KJ1600407, KJQN201900601), and Natural Science Foundation of Chongqing.

References

[1] R Benzi, G Parisi, A Sutera and A Vulpiani *Tellus* **34** 10 (1982)
[2] R Benzi *Nonlinear Processes in Geophysics* **17** 431 (2010)
[3] L F He, Y L Yang and T Q Zhang *Chinese Journal of Scientific Instrument* **40** 47 (2019)
[4] J M Liu, J Mao, B Huang and P G Liu *Physics Letters A* **382** 3071 (2018)
[5] Z J Qiao, Y G Lei, J Lin and S T Niu *Physical Review E* **94** 052214 (2016)
[6] Q Y Wang, H H Zhang and G R Chen *Chaos An Interdisciplinary Journal of Nonlinear Science* **22** 043123 (2012)
[7] H T Yu, J Wang, J W Du, B Deng, X L Wei and C Liu *Chaos An Interdisciplinary Journal of Nonlinear Science* **23** 013128 (2013)
[8] S L Lu, Q B He and F R Kong *Digital Signal Processing* **36** 93 (2015)
[9] G Zhang, Y J Zhang, T Q Zhang and M Rana *Chinese Journal of Physics* **56** 1173 (2018)
[10] P M Shi, Q Li and D Y Han *Chinese Journal of Physics* **54** 526 (2016)
[11] M J He, W Xu and Z K Sun *Nonlinear Dynamics* **79** 1787 (2015)
[12] S B Jiao, R Yang, Q Zhang and G Xie *Acta Physica Sinica* **64** 20502 (2015)
[13] M A Fuentes, R Toral and H S Wio *Physica A: Statistical Mechanics and its Applications* **295** 114 (2001)
[14] Y F Jin and B Li *Acta Physica Sinica* **63** 210501 (2014)
[15] Y F Guo, Y J Shen and J G Tan *Communications in Nonlinear Science and Numerical Simulation* **38** 257 (2016)
[16] G Zhang, D Y Hu and T Q Zhang *Chinese Journal of Physics* **56** 2718 (2018)
[17] Y F Guo, B Xi, F Wei and J G Tan *Modern Physics Letters B* **32** 1850339 (2018)
[18] S H Li and J Huang *AIP Advances* **10** 025310 (2020)
[19] L F He, C L Tan and G Zhang *The European Physical Journal Plus* **136** 1 (2021)
[20] G Zhang, C Jiang and T Q Zhang *Fluctuation and Noise Letters* **20** 2150004 (2021)
[21] P M Shi, W Y Zhang, D Y Han and M D Li *Chaos Solitons & Fractals* **128** 155 (2019)
[22] P F Xu and Y F Jin *Applied Mathematical Modelling* **77** 408 (2020)
[23] W Y Zhang, P M Shi, M D Li, Y X Mao and D Y Han *IEEE Access* **7** 173753 (2019)
[24] H S Wio and R Toral *Physica D: Nonlinear Phenomena* **193** 161 (2004)